Journal of Materials Chemistry A

Accepted Manuscript

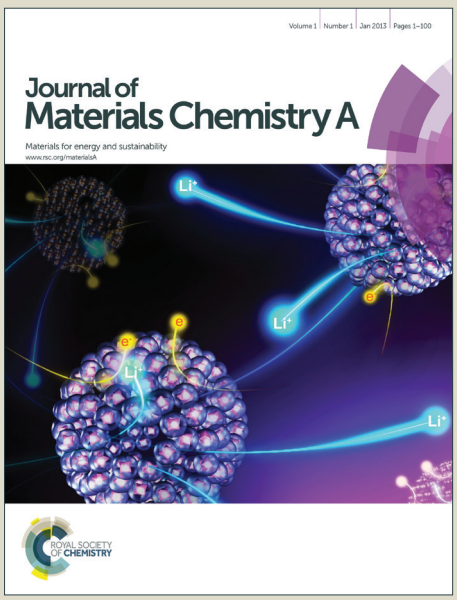

ROYAL SOCIETY OF CHEMISTRY

www.rsc.org/materialsA

Journal Name

COMMUNICATION

Facile synthesis of nitrogen-doped carbon nanosheets with hierarchical porosity for high performance supercapacitors and lithium-sulfur batteries

Received 00th January 20xx,
Accepted 00th January 20xx

DOI: 10.1039/x0xx00000x

www.rsc.org/

Xiaoliang Yu,[ac] Jianfeng Zhao,[b] Ruitao Lv,[b] Qinghua Liang,[b] Changzhen Zhan,[b] Yu Bai,[b] Zheng-Hong Huang, *[ab] Wanci Shen,[b] Feiyu Kang*[b]

Magnesium citrate and potassium citrate are two commonly used food additives in our daily life. Herein, we prepared nitrogen-doped hierarchical porous carbon nanosheets (N-HPCNS) through direct pyrolysis of their mixtures and subsequent NH_3 treatment. As-prepared N-HPCNS shows a hierarchical porosity (specific surface area of 1735 $m^2 g^{-1}$ and pore volume of 1.71 $cm^3 g^{-1}$), and a moderate nitrogen doping of 1.7%. Moreover, it can be effectively applied in various energy storage/conversion systems. When used for supercapacitor electrodes, it shows a high specific capacitance of 128 F g^{-1} in organic electrolyte which retains 45% even at an ultrahigh current density of 100 A g^{-1}. It can also serve as an effective sulfur carrier in lithium-sulfur batteries. The N-HPCNS/sulfur cathode shows high discharge capacities of 1209 mAh g^{-1} at 0.2 C and 493 mAh g^{-1} even at 4 C. Over 500 charge/discharge cycles at 1 C, it still remains a high discharge capacity of 486 mAh g^{-1} with an ultralow capacity loss of 0.051% per cycle and a high average Coulombic efficiency of 99.4%.

The Electrochemical energy storage (EES) has attracted tremendous attention due to the ever-increasing demand for alleviating urgent energy and environmental issues. Among various EES technologies, supercapacitor and lithium-sulfur (Li-S) battery are two promising candidates. Supercapacitor can achieve high power delivery by fast ion adsorption/desorption at the electrode/electrolyte interface,[1] while Li-S battery enables high energy storage through multi-step redox reactions between lithium and sulfur.[2] To obtain excellent electrochemical performance in two EES systems, the exploration of advanced electrode materials is the key point.

Two-dimensional (2D) nanostructured carbon materials are being extensively explored for next-generation ESS systems. Also 2D porous carbons have received special attentions. Their open porous and layered structure results in good electrolyte accessibility and short diffusion distance. Besides, they also enable facile strain relaxation during battery operation.[3] Thus significantly enhanced electrochemical performance can be achieved in comparison with the bulk materials. Various synthetic strategies have been developed to prepare 2D porous carbons.[4-16] And graphene oxide-directed synthesis has been the most widely employed method. Graphene oxide can serve as an effective 2D matrix for in-situ polymerization. After subsequent pyrolysis, 2D porous carbon can be achieved.[7] To further improve the porosity in such synthesis processes, introduction of templates or post chemical activation can be emploáyed.[8-11] In addition, biomass derived materials were reported to be effective precursors to prepare 2D porous carbons. Wang *et al.* prepared highly porous interconnected carbon nanosheets in a two-step procedure that involves the carbonization of hemp and following chemical activation.[12] Qiu *et al.* synthesized 2D porous carbon by an integrated procedure of intercalation, pyrolysis, and activation.[13] However, all these above-mentioned synthesis strategies are somewhat complex and may cause severe equipment corrosion. Recently, some researchers reported facile synthesis of 2D porous carbons through co-pyrolysis of phenolic resin and copper nitrate,[14] ferrocene and carbon disulfide,[15] or direct pyrolysis of potassium citrate.[16] Unfortunately, the achieved porous carbon nanosheets exhibit quite low porosity or dominantly microporosity, which are not appropriate for high-power supercapacitor and Li-S battery applications.

In recent years, the design of porous carbons with hierarchical porosity is another research focus in supercapacitor and Li-S battery applications.[17-20] The micropores and small mesopores provide confinement for electrolyte ions or sulfur molecules to store energy, while the large mesopores and macropores offer smooth pathways for mass transport. Thus both large specific capacity and good high-rate capability can be achieved. Further, the heteroatom incorporation has been reported to be a very efficient approach to improve the electrochemical performance in both applications. In supercapacitors, certain nitrogen doping can enhance the surface wettability of porous carbon electrodes in electrolyte and the electric conductivity of porous carbon framework.[21-23] In Li-S batteries, nitrogen-doping not only improves the carbon wettability and conductivity, but also provides a strong adsorption on sulfur

[a] *State Key Laboratory of New Ceramics and Fine Processing, School of Materials Science and Engineering, Tsinghua University, Beijing 100084, China.*
[b] *Key Laboratory of Advanced Materials (MOE), School of Materials Science and Engineering, Tsinghua University, Beijing 100084, China.*
[c] *Engineering Laboratory for Functionalized Carbon Materials, Graduate School at Shenzhen, Tsinghua University, Shenzhen 518055, China.*
Email: zhhuang@tsinghua.edu.cn (Z.-H Huang); fykang@tsinghua.edu.cn (F. Kang).

† Electronic Supplementary Information (ESI) available. See DOI: 10.1039/x0xx00000x

and lithium polysulfides, resulting in enhanced sulfur utilization and cycle life of the carbon/sulfur composites.[24-26]

For these reasons, developing a facile and scalable method to prepare novel nitrogen-doped 2D porous carbon with hierarchical porosity is urgently demanded. Magnesium citrate is a commonly used food additive, and Inagaki firstly reported that it can serve as both carbon source and hard template to prepare mesoporous carbon.[27] Here, inspired by this synthesis method and the high effectiveness of potassium ions in the synthesis of carbon nanosheet,[10-12, 16, 28] we performed co-pyrolysis of magnesium citrate and potassium citrate and following NH_3 treatment. As a result, nitrogen-doped hierarchical porous carbon nanosheets (N-HPCNS) were prepared, which exhibit superior performances in supercapacitor and Li-S battery applications. The mass ratio of magnesium citrate to potassium citrate is controlled to be 4:1 for the synthesis of N-HPCNS. The detailed description of material synthesis and characterization can be seen in the experimental section in the ESI†. For reference, potassium citrate was individually employed as the raw material to prepare nitrogen-doped microporous carbon nanosheets (N-MPCNS). Magnesium citrate and the mixture with a mass ratio of 8:1 were also separately employed as raw materials to prepare two kinds of nitrogen-doped hierarchical porous carbons (designated as N-HPC1 and N-HPC2, respectively).

Fig 1 and Fig. S2 show the SEM and TEM images of four porous carbons. Sample N-HPC1 derived from magnesium citrate shows an irregular bulk morphology with particle sizes from 2 to 10 μm (Fig. S2a). From the corresponding TEM image (Fig. S2b) we can observe mesopores with uneven pore sizes from 10 to 20 nm, which should be derived from the removal of MgO nanocrystals. With the introduction of potassium citrate, sample N-HPC2 shows some individual carbon nanosheets extending from the carbon framework (Fig. S2c). And remarkably more obvious mesopores can be observed in the TEM image (see Fig. S2d). As the potassium citrate content increases, sample N-HPCNS shows large quantity of individual carbon nanosheets with thickness of 100-200 nm (Fig. 1a). From the corresponding TEM image in Fig 1b we can observe clearly plenty of large mesopores throughout the nanosheets, confirming its thin layered structure. From Fig. 1c we can see that sample N-MPCNS derived from only potassium citrate shows an interconnected network of carbon nanosheets, and no obvious mesopores can be observed in the TEM image (Fig. 1d).

Nitrogen adsorption tests were undertaken to characterize the texture properties of the sheet-like porous carbons before and after NH_3 treatment, and the results are shown in Fig. 1 and Fig. S3. N-HPCNS exhibits a hybrid of type-I and type-IV isotherm (see Fig. 1e), indicating its hierarchical porous structure combining micro- and mesopores. While N-MPCNS presents a typical type-I isotherm indicating its dominant micropore structure. From the corresponding pore size distributions in Fig. 1f, we can see that N-HPCNS shows a much more developed mesoporosity with trimodal distributions centered at 2.6 nm, 7.8 nm and 13.4 nm. The micropores and small mesopores (2.6 nm) of sample N-HPCNS come from the thermal decomposition of the carbon matrix, while the large mesopores should be ascribed to the removal of MgO nanocrystals. The porosity parameters of various porous carbons are summarized in Table S1. The high specific surface area of sample N-HPCNS (1735 $m^2 g^{-1}$) is comparable to that of N-MPCNS (1776 $m^2 g^{-1}$). And its large pore volume (1.71 $cm^3 g^{-1}$) is much superior to that of N-MPCNS (1.07 $cm^3 g^{-1}$). We can also find that NH_3 treatment causes minor change of the porous structure, with little enhancement of specific surface areas and pore volumes, and almost no change of the pore size distributions. According to the microstructure evolution among different porous carbons, we schematically illustrated the generative process of sample N-HPCNS in Fig. 1g. Firstly during pyrolysis, the organic moiety polymerized and then further carbonized to form the carbon framework, and the magnesium and potassium ions nucleated to form nanocrystals of MgO and K_2O. Secondly, K_2O reacted with carbon framework to form metallic potassium ($K_2O+C \rightarrow 2K+CO$) and produce plenty of micropores. Then potassium vapors further etched the carbon framework. Due to the existence of large quantity of MgO nanocrystals, the carbon walls become quite thin and easy to be etched. Thus some individual carbon nanosheets extending from the carbon framework were generated. Thirdly, potassium vapors continued to etch the carbon framework to produce more and more individual carbon nanosheets. Following acid washing removed MgO nanocrystals to generate large quantity of mesopores. After subsequent NH_3 treatment, nitrogen-doped carbon nanosheets with hierarchical porosity can be achieved. XPS analysis were carried out to evaluate the surface chemistry of porous carbons and the results are shown in Fig. S4. Signals of N and O elements can be observed, and nitrogen contents of 1.7% and 1.8% can be determined for N-HPCNS and N-MPCNS based on the XPS quantitative analysis. Such moderate nitrogen functional groups are quite beneficial for improving the polarity and wettability of the porous surface as well as enhancing the electric conductivity.[29, 30]

Since N-HPCNS shows appropriate characteristics for high-performance supercapacitors, like a hierarchical porosity, a moderate nitrogen doping and a layered structure with short diffusion paths, here we employed N-HPCNS as the electrode material to assemble symmetric supercapacitors. Its capacitive performances were investigated in detail and the results are shown in Fig. 2. Sample N-MPCNS was also tested for reference. Fig. 2a shows the cyclic voltammetry (CV) curves of N-HPCNS at various scan rates. The CV curves exhibit nearly rectangular shapes, which are well retained even at high scan rate (100 mV s^{-1}), demonstrating its fast ion transport at high charge/discharge rate and ideal capacitive behavior.[31] Whereas, the CV curves of N-MPCNS shows some distortion at high scan rates (Fig. S5), which should be ascribed to the lack of mesopore diffusion channels and thus slower ion transport at high rate operations.[32, 33] A high specific capacitance of 130 F g^{-1} was calculated according to the CV test at 10 mV s^{-1}, and it remains 121 F g^{-1} at 100 mV s^{-1}. Galvanostatic charge/discharge tests were also conducted. Fig. 2b shows galvanostatic charge/discharge curves with isosceles triangle shapes, again suggesting the electric-double-layer capacitive feature. The specific capacitances of two porous carbons at various current densities were calculated and plotted in Fig. 2c. At a low current density of 0.1 A g^{-1}, N-HPCNS shows a high specific capacitance of 128 F g^{-1}, which is in accordance with the results of CV tests. At an ultrahigh current density of 100 A g^{-1}, it still retains 45% of the original capacitance. N-MPCNS shows a specific

capacitance of 135 F g^{-1} at 0.1 A g^{-1}, which maintains only 21% at 40 A g^{-1}. The huge rate performance gap between N-HPCNS and N-MPCNS demonstrates the great advantage of the hierarchical porous structure for fast ion transport. Fig. S6 shows the relationship between energy density and power density, also known as Ragone plot of the symmetric supercapacitor based on the N-HPCNS electrodes. It shows a high energy density of 32.4 Wh kg^{-1} at 73 W kg^{-1}. At an ultrahigh power density of 75 kW kg^{-1}, it still maintains an energy density of 14.6 Wh kg^{-1}. This high-power performance outperforms those of many previously reported porous carbons (see Fig. S6). Fig. 2d shows the cyclic stability of two samples. After 5000 charge/discharge cycles at a current density of 5 A g^{-1}, N-HPCNS still retains 86.8% of its original capacitance, indicating its good cycling performance.

In this work, we also impregnate sulfur into N-HPCNS to prepare N-HPCNS/sulfur (N-HPCNS/S) cathode for Li-S batteries. For reference, N-MPCNS/sulfur (N-MPCNS/S) composite was prepared by the same method. Fig. S7 shows the thermogravimetric analysis (TGA) curves of as-obtained two composites. The sulfur contents can be determined to be 59.8 wt% and 58.8 wt% for N-HPCNS/S and N-MPCNS/S, respectively. In order to evaluate the sulfur dispersability in two composites, TEM tests were performed and the TEM images are shown in Fig. S8. We can find no discernible sulfur particles indicating the highly dispersed state of sulfur inside the porous carbons. This is in good agreement with their XRD patterns shown in Fig. S9. The carbon/sulfur (C/S) composites do not show the diffraction peaks in sublimed sulfur, again implying the good dispersability of sulfur in the carbon matrixes. Nitrogen adsorption tests were performed to evaluate the texture properties of C/S composites (see Fig. S10). After sulfur impregnation, the porosities especially the micro- and small mesoporosities of C/S composites were enormously reduced in comparison with corresponding porous carbons.

To evaluate the electrochemical performance of C/S composites, coin cells employing lithium foil as an anode and the C/S composite as a cathode were assembled. Fig. 3a plots voltages *vs.* specific capacities for the N-HPCNS/S cathode at a charge/discharge rate of 0.2 C. Two discharge plateaus and one charge plateau respectively corresponding to the electrochemical reduction and oxidation of sulfur can be seen. The higher discharge plateaus at 2.25 V is related to the conversion of sulfur to long chain lithium polysulfides (Li_2S_n, $4 \le n \le 8$), and the low discharge plateaus at 2.1 V corresponds to the reduction of lithium polysulfides to Li_2S_2 or Li_2S. The charge plateau at 2.35 V is assigned to the oxidation of Li_2S_2 or Li_2S to high-order lithium polysulfide.[34] Fig. 3b shows the specific capacities at various charge/discharge rates from 0.2 C to 4 C for two C/S cathodes. N-HPCNS/S cathode shows a high discharge capacity of 1205 mAh g^{-1} at 0.2 C, which is 72.2% of the theoretical value (1675 mAh g^{-1}) and a little higher than that of N-MPCNS/S cathode (1168 mAh g^{-1}). Even at a charge/discharge rate as high as 4 C, it still maintains 493 mAh g^{-1} which is more than twice that of N-MPCNS/S cathode (242 mAh g^{-1}), indicating its good high-rate performance. This excellent rate performance could be attributed to several factors. Firstly, the nitrogen-doped carbon matrix greatly facilitates the electron conduction in C/S composite. Secondly, the highly dispersed sulfur could contact well with the carbon matrix and thus provide high electrochemical activity during charge/discharge. Thirdly, the layered structure enables a short diffusion length. Last and most importantly, the hierarchical porous structure provide smooth channels for ion diffusions, which is also the main reason for the rate performance gap between two C/S cathodes. Fig. 3c shows the electrochemical impedance spectroscopy (EIS) plots of two C/S cathodes. The intercept of the semicircle with the real axis represents the electric resistance (R_e) of the Li-S cell. The semicircle could be related to the charge transfer process at the electrode/electrolyte interface, and its diameter represents the charge transfer resistance (R_{ct}). We can observe that both R_e and R_{ct} values of N-HPCNS are lower than those of N-MPCNS. Thus it can be suggested that N-HPCNS is a better sulfur carrier in Li-S battery. Fig. 3d shows the cycling stability of the C/S composites at a charge/discharge rate of 1 C. The N-HPCNS/S cathode shows an initial discharge capacity of 652 mAh g^{-1}, which is much higher than 480 mAh g^{-1} for N-MPCNS/S. After 500 charge/discharge cycles, N-HPCNS/S still remains a high discharge capacity of 486 mAh g^{-1} with 74.5% capacity retention and an average Coulombic efficiency of 99.4%. It is worth mentioning that the capacity loss per cycle is as low as 0.051%, which is among the best reported cycling performances in literatures.[35-38] This superior cycling stability should be ascribed to the strong physical adsorption from micro- and small mesopores as well as the chemical adsorption from nitrogen heteroatoms.

Conclusions

In conclusion, we have prepared nitrogen-doped hierarchical porous carbon nanosheets (N-HPCNS) through facile co-pyrolysis of magnesium citrate and potassium citrate with a mass ratio of 4:1 and subsequent NH_3 treatment. As-obtained N-HPCNS can be effectively employed in both supercapacitor and Li-S battery applications. When used for supercapacitor, it shows a high specific capacitance of 128 F g^{-1} in organic electrolyte, and maintains 45% of the capacitance even at an ultrahigh current density of 100 A g^{-1}. In Li-S battery applications, the N-HPCNS/S cathode shows high discharge capacities of 1209 mAh g^{-1} at 0.2 C and 493 mAh g^{-1} even at 4 C. And it remains 486 mAh g^{-1} over 500 charge/discharge cycles at 1 C, with an ultralow capacity loss of 0.051% per cycle and a high average Coulombic efficiency of 99.4%. Considering the low cost of raw materials and facile scalable processes, this work features a promising approach to prepare nitrogen-doped 2D porous carbons with hierarchical porosity for applications in high-performance supercapacitors and Li–S batteries.

Acknowledgements

The authors gratefully thank the National Natural Science Foundation of China (Grant No. 51232005), 973 program of China (No.2014CB932401) for the financial support.

Notes and references

1 L. Zhang and X. Zhao, *Chem. Soc. Rev.*, 2009, 38, 2520-2531.
2 X. Ji, K. T. Lee and L. F. Nazar, *Nat. Mater.*, 2009, 8, 500-506.
3 J. Liu and X. W. Liu, *Adv. Mater.*, 2012, 24, 4097-4111.

4 Y. Fang, Y. Lv, R. Che, H. Wu, X. Zhang, D. Gu, G. Zheng and D. Zhao, *J. Am. Chem. Soc.*, 2013, 135, 1524-1530.
5 Y. Qian, I. M. Ismail and A. Stein, *Carbon*, 2014, 68, 221-231.
6 J. Huang, J. Wang, C. Wang, H. Zhang, C. Lu and J. Wang, *Chem. Mater.*, 2015, 27, 2107-2113.
7 G.-P. Hao, Z.-Y. Jin, Q. Sun, X.-Q. Zhang, J.-T. Zhang and A.-H. Lu, *Energy Environ. Sci.*, 2013, 6, 3740-3747.
8 X. Zhuang, F. Zhang, D. Wu and X. Feng, *Adv. Mater.*, 2014, 26, 3081-3086.
9 W. Wei, H. Liang, K. Parvez, X. Zhuang, X. Feng and K. Müllen, *Angew. Chem. Int. Ed.*, 2014, 126, 1596-1600.
10 H. g. Wang, Z. Wu, F. l. Meng, D. l. Ma, X. l. Huang, L. m. Wang and X. b. Zhang, *ChemSusChem*, 2013, 6, 56-60.
11 Q. Wen, S. Wang, J. Yan, L. Cong, Y. Chen and H. Xi, *Bioelectrochemistry*, 2014, 95, 23-28.
12 H. Wang, Z. Xu, A. Kohandehghan, Z. Li, K. Cui, X. Tan, T. J. Stephenson, C. K. King'ondu, C. M. Holt and B. C. Olsen, *ACS Nano*, 2013, 7, 5131-5141.
13 X. Fan, C. Yu, J. Yang, Z. Ling, C. Hu, M. Zhang and J. Qiu, *Adv. Energy Mater.*, 2015, 5: 1401761. doi: 10.1002/aenm.201401761.
14 R. Song, H. Song, J. Zhou, X. Chen, B. Wu and H. Y. Yang, *J. Mater. Chem.*, 2012, 22, 12369-12374.
15 J.-M. Shen and Y.-T. Feng, *J. Phys. Chem. C*, 2008, 112, 13114-13120.
16 M. Sevilla and A. B. Fuertes, *ACS Nano*, 2014, 8, 5069-5078.
17 D. W. Wang, F. Li, M. Liu, G. Q. Lu and H. M. Cheng, *Angew. Chem. Int. Ed.*, 2008, 120, 379-382.
18 Y. Lv, L. Gan, M. Liu, W. Xiong, Z. Xu, D. Zhu and D. S. Wright, *J. Power Sources*, 2012, 209, 152-157.
19 B. Ding, C. Yuan, L. Shen, G. Xu, P. Nie and X. Zhang, *Chem.–Eur. J.*, 2013, 19, 1013-1019.
20 K. Xi, S. Cao, X. Peng, C. Ducati, R. V. Kumar and A. K. Cheetham, *Chemical Commun.*, 2013, 49, 2192-2194.
21 Z. Wen, X. Wang, S. Mao, Z. Bo, H. Kim, S. Cui, G. Lu, X. Feng and J. Chen, *Adv. Mater.*, 2012, 24, 5610-5616.
22 L.-F. Chen, X.-D. Zhang, H.-W. Liang, M. Kong, Q.-F. Guan, P. Chen, Z.-Y. Wu and S.-H. Yu, *ACS Nano*, 2012, 6, 7092-7102.
23 X. Yu, C. Zhan, R. Lv, Y. Bai, Y. Lin, Z.-H. Huang, W. Shen, X. Qiu and F. Kang, *Nano Energy*, 2015, 15, 43-53.
24 X. G. Sun, X. Wang, R. T. Mayes and S. Dai, *ChemSusChem*, 2012, 5, 2079-2085.
25 F. Sun, J. Wang, H. Chen, W. Li, W. Qiao, D. Long and L. Ling, *ACS Appl. Mater. Interfaces*, 2013, 5, 5630-5638.
26 Y. Qiu, W. Li, W. Zhao, G. Li, Y. Hou, M. Liu, L. Zhou, F. Ye, H. Li and Z. Wei, *Nano Lett.*, 2014, 14, 4821-4827.
27 M. Inagaki, M. Kato, T. Morishita, K. Morita and K. Mizuuchi, *Carbon*, 2007, 45, 1121-1124.
28 J. Ding, H. Wang, Z. Li, A. Kohandehghan, K. Cui, Z. Xu, B. Zahiri, X. Tan, E. M. Lotfabad and B. C. Olsen, *ACS Nano*, 2013, 7, 11004-11015.
29 Z. S. Wu, A. Winter, L. Chen, Y. Sun, A. Turchanin, X. Feng and K. Müllen, *Adv. Mater.*, 2012, 24, 5130-5135.
30 J. Liang, X. Du, C. Gibson, X. W. Du and S. Z. Qiao, *Adv. Mater.*, 2013, 25, 6226-6231.
31 W. Zhang, Z.-H. Huang, C. Zhou, G. Cao, F. Kang and Y. Yang, *J. Mater. Chem.*, 2012, 22, 7158-7163.
32 L. Sun, C. Tian, M. Li, X. Meng, L. Wang, R. Wang, J. Yin and H. Fu, *J. Mater. Chem. A*, 2013, 1, 6462-6470.
33 Z. Fan, Y. Liu, J. Yan, G. Ning, Q. Wang, T. Wei, L. Zhi and F. Wei, *Adv. Energy Mater.*, 2012, 2, 419-424.
34 Y.-S. Su, Y. Fu, T. Cochell and A. Manthiram, *Nat. Commun.*, 2013, 4, 2985-2992.
35 X. Yang, L. Zhang, F. Zhang, Y. Huang and Y. Chen, *ACS Nano*, 2014, 8, 5208-5215.
36 H.-J. Peng, J. Liang, L. Zhu, J.-Q. Huang, X.-B. Cheng, X. Guo, W. Ding, W. Zhu and Q. Zhang, *ACS Nano*, 2014, 8, 11280-11289.
37 Y. Huang, M. Zheng, Z. Lin, B. Zhao, S. Zhang, J. Yang, C. Zhu, H. Zhang, D. Sun and Y. Shi, *J. Mater. Chem. A*, 2015, 3, 10910-10918.
38 Z. Zhang, H.-K. Jing, S. Liu, G.-R. Li and X.-P. Gao, *J. Mater. Chem. A*, 2015, 3, 6827-6834.

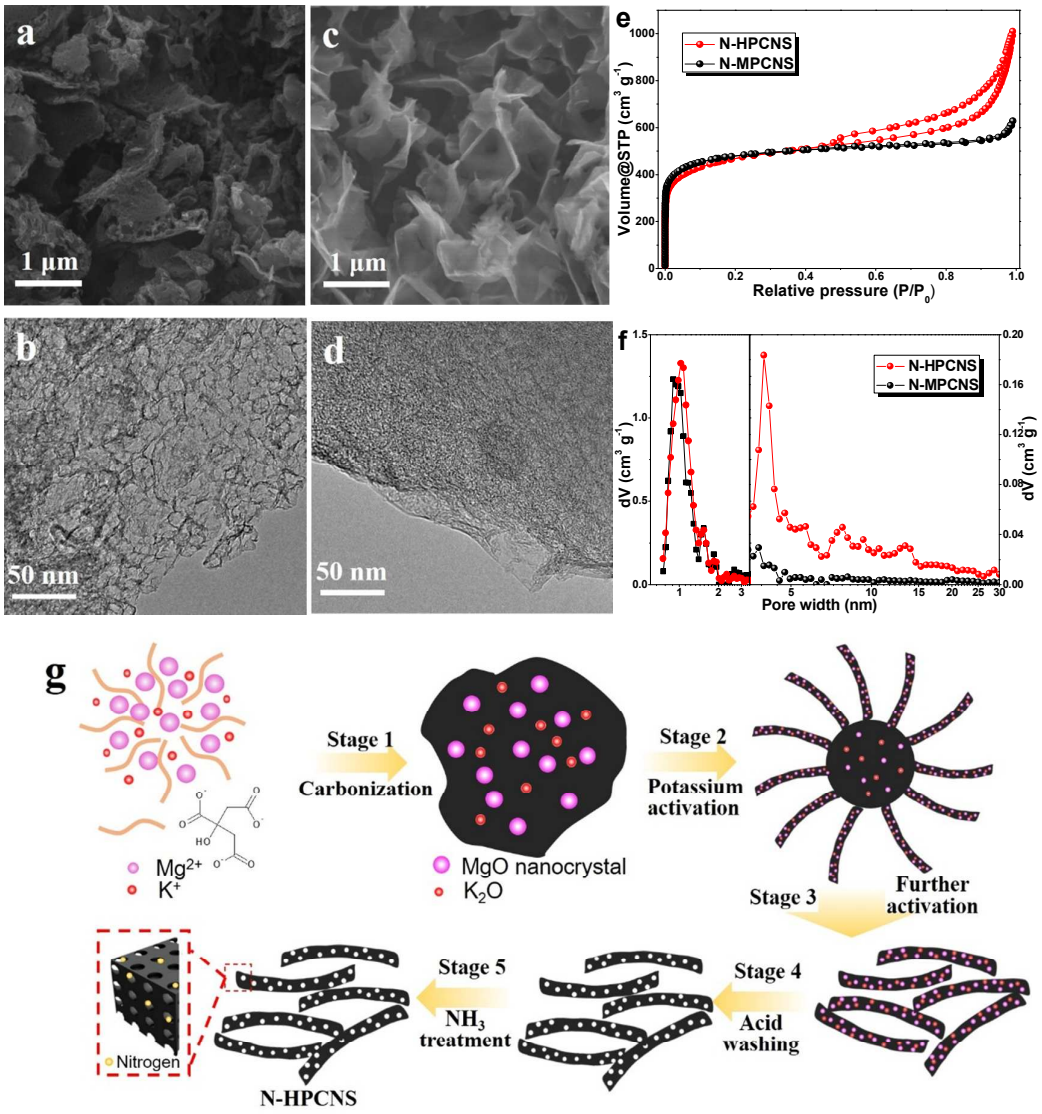

Fig.1 SEM and TEM images of N-HPCNS (a, b), N-MPCNS (c, d); nitrogen adsorption isotherms of N-HPCNS and N-MPCNS (e), and their corresponding pore size distributions (f); schematic diagram for the formation process of N-HPCNS (g).

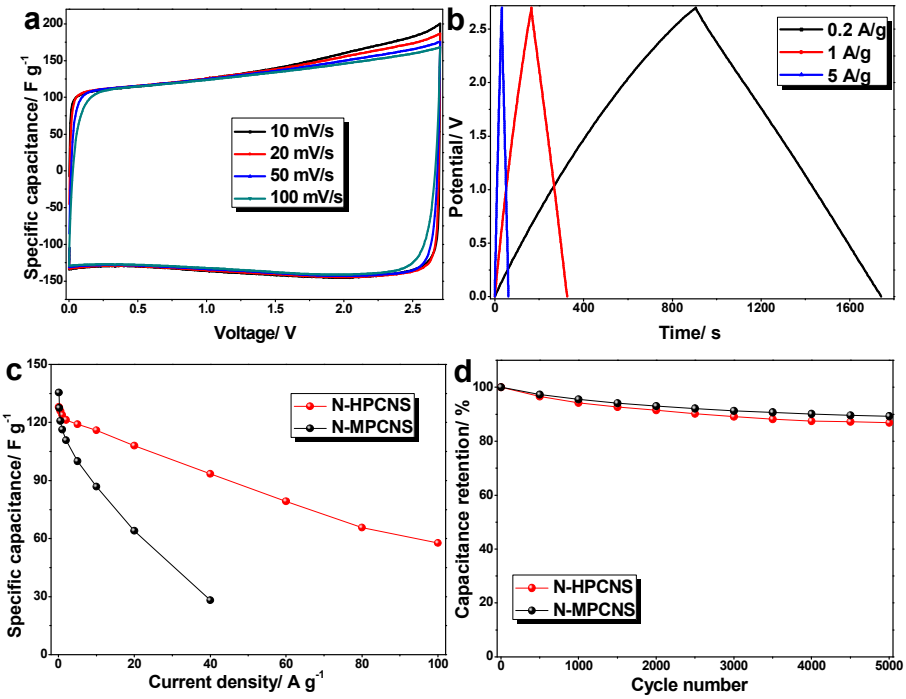

Fig. 2 (a) CV curves at various scan rates for N-HPCNS, (b) GC curves at various current densities for N-HPCNS, (c) rate performances and (d) cycling stability of N-HPCNS and N-MPCNS.

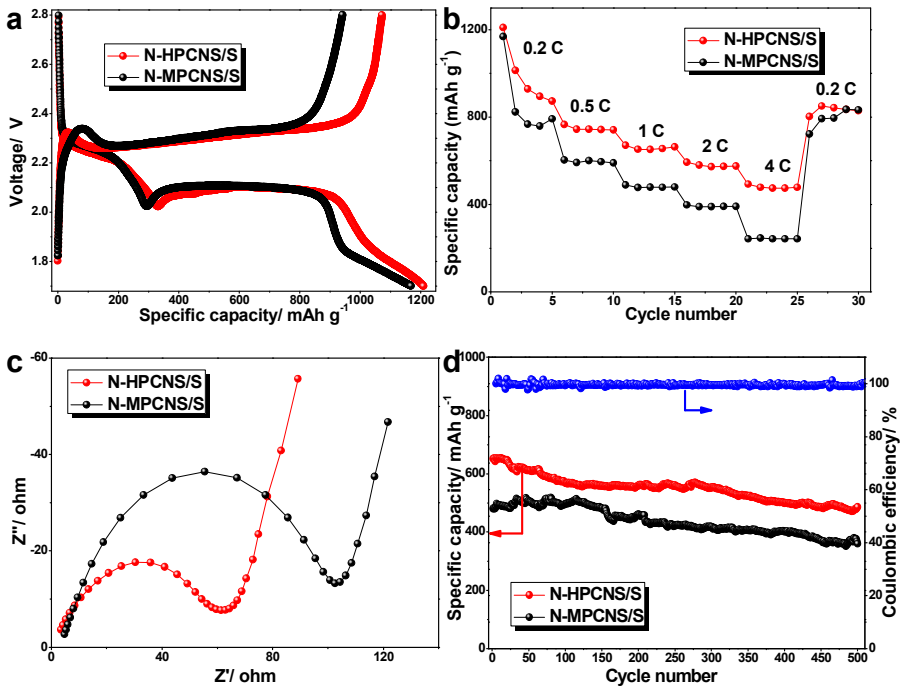

Fig. 3 (a) Charge/discharge curves of N-HPCNS/S and N-MPCNS/S cathodes at a current density of 0.2 C, (b) rate performances, (c) EIS plots, and (d) cycling stability of two cathodes.

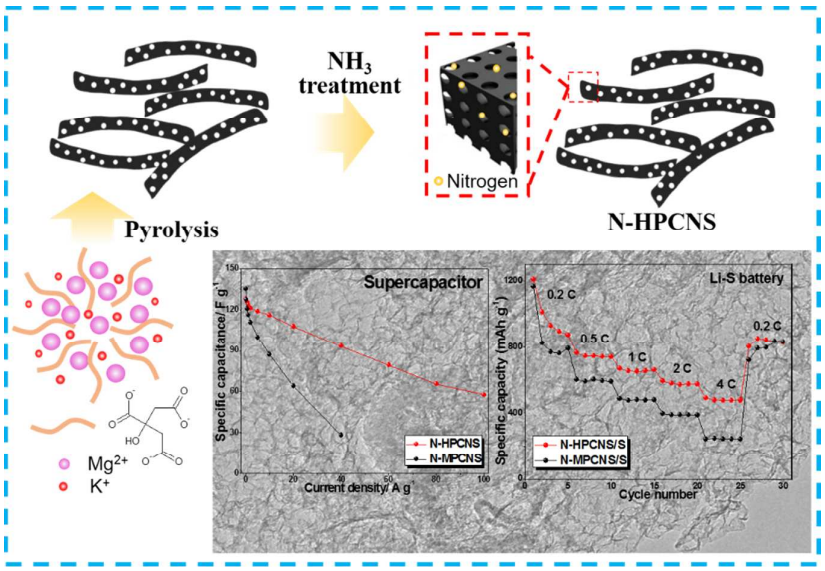

Nitrogen-doped hierarchical porous carbon nanosheets were prepared through co-pyrolysis of magnesium citrate and potassium citrate and following NH_3 treatment.